Communications in Physics, Vol. 36, No. 1 (2026), pp. 27-36
DOI: https://doi.org/10.15625/0868-3166/23333

Polarization-selective electromagnetically induced transparency in asymmetric mid-infrared plasmonic metamaterials

The Linh Pham[1], **Nguyen Hai Anh**[2,3], **Nguyen Thi Mai**[2], **Vu Dinh Lam**[3], **Ewald Janssens**[1,†] **and Nguyen Thanh Tung**[2,3,‡]

[1]*Quantum Solid-State Physics, Department of Physics and Astronomy, KU Leuven, Celestijnenlaan 200D, Leuven 3001, Belgium*

[2]*Institute of Materials Science, Vietnam Academy of Science and Technology, 18 Hoang Quoc Viet, Nghia Do, Hanoi, Vietnam*

[3]*Graduate University of Science and Technology, Vietnam Academy of Science and Technology, 18 Hoang Quoc Viet, Nghia Do, Hanoi, Vietnam*

E-mail: [†]ewald.janssens@kuleuven.be; [‡]tungnt@ims.vast.ac.vn

Received 19 August 2025; *Accepted for publication 12 November 2025*
Published 5 March 2026

Abstract. *We demonstrate polarization-controlled electromagnetically induced transparency in asymmetric H-shaped plasmonic metamaterials operating in the mid-infrared regime (6-12 μm). Through controlled symmetry breaking of coupled gold cut-wire resonators, we achieve strong coupling between bright (superradiant) and dark (subradiant) modes, evidenced by an anti-crossing behavior in the reflectance spectrum. Fourier-transform infrared spectroscopy reveals a tunable transparency window with up to 55% reflectance suppression under transverse electric polarization, while a single plasmonic resonance is maintained under transverse magnetic-polarized excitation. Finite-integration technique simulations and field distribution analysis confirm the hybridized nature of the observed states, showing quadrupole-dipole mode interaction. The polarization-selective electromagnetically induced transparency response emerges from coupling between vertical and horizontal resonators whose coupling strength is systematically controlled via lateral displacement (0-0.2 μm) of the vertical resonator. This work establishes a robust platform for tunable mid-infrared photonics, bridging quantum-inspired phenomena with practical metamaterial design for applications in molecular sensing, active optical components, and quantum plasmonics.*

Keywords: infrared; metamaterials; plasmonic; strong coupling; electromagnetically induced transparency.

Classification numbers: 42.70.Km; 81.05.Xj; 78.67.Pt; 91.25.Qi.

1. Introduction

Plasmonics, the study of electromagnetic interactions between light and free electrons in metallic nanostructures, has emerged as a transformative field in nanophotonics, enabling control of light at subwavelength scales [1]. Metamaterials, artificial structures engineered with tailored optical properties, have further expanded this paradigm by facilitating phenomena such as negative refraction, cloaking, and enhanced light-matter interactions [2,3]. Among the most intriguing plasmonic phenomena is strong coupling, where localized surface plasmon resonances interact coherently with other resonances, leading to hybridized modes and effects like electromagnetically induced transparency (EIT) [4]. EIT effects, characterized by a narrow transparency window within a broad absorption band, arise from the interplay between bright (superradiant) and dark (subradiant) modes, offering potential applications in sensing, nonlinear optics, and quantum plasmonics [5, 6].

Recent advances in plasmonics have significantly deepened understanding of strong coupling. In the visible and near-infrared regimes, researchers have demonstrated EIT effects in coupled plasmonic systems, such as nanoparticle arrays, split-ring resonators, and metasurfaces [7–9]. For instance, Liu *et al.* reported strong coupling in gold nanorod dimers, achieving Rabi splitting energies exceeding 100 meV [7]. Similarly, advances in fabrication techniques, such as electron-beam lithography and self-assembly, have enabled precise control over subwavelength structures, which allowed one to enhance coupling strengths [10]. Computational methods, including finite-difference time-domain (FDTD) and finite-integration technique (FIT) simulations, have further elucidated mode hybridization and dispersion [11]. Moreover, the integration of plasmonic systems with two-dimensional materials (e.g., graphene) and quantum emitters has opened new avenues for tunable and quantum-enhanced plasmonics [12, 13].

Despite these breakthroughs, most studies have been restricted to visible, near-infrared and microwave wavelengths, while their extension to the mid-infrared (mid-IR, 2.5–25 μm) has been studied less due to challenges in achieving low-loss plasmonic resonances, high-quality plasmonic resonances [14] and scalable fabrication. Nonetheless, the mid-IR regime, which aligns with vibrational modes of molecules, presents a compelling frontier for plasmonic research due to its relevance in molecular spectroscopy, sensing application, thermal imaging, and on-chip photonics [15, 16]. Extending EIT effects to the mid-infrared is critical to validate the universality of strong coupling across spectral regimes and to unlock applications in infrared photonics, where current technologies lag behind their visible counterparts [17]. Recent studies, such as those by Bejide *et al.* and Han *et al.*, have demonstrated mid-infrared optical modulators using metasurfaces [18, 19], but systematic investigations of strong coupling and mode hybridization remain limited [20–23].

Here, we experimentally demonstrate polarization-selective EIT in mid-IR metamaterials through controlled symmetry breaking. Using H-shaped gold resonators on a silicon substrate, we engineer strong coupling between orthogonal plasmonic modes, achieving a tunable transparency window with a strong reflectance suppression under transverse electric (TE) polarization while maintaining a single resonance under transverse magnetic (TM) excitation. Finite-integration technique (FIT) simulations and Fourier-transform infrared (FTIR) spectroscopy reveal that lateral displacement of resonator elements (0–0.2 μm) systematically modulates the coupling strength,

enabling the transition to the strong coupling regime. These findings provide a blueprint for designing active mid-IR photonic devices that combine the spectral agility of quantum systems with the scalability of classical metamaterials.

2. Experiment and simulation

The metamaterial samples were fabricated using electron-beam lithography and sputtering deposition techniques. A silicon substrate (intrinsic, two-side polished and 800 μm thick) was first cleaned using standard protocols before spin-coating with polymethyl methacrylate (PMMA) photoresist at 4000 rpm for 60 seconds, resulting in an approximately 200 nm thick resist layer. Electron-beam lithography was performed using a Raith eLINE Plus system operating at 20 kV with a dose of 300 μC/cm^2. The exposed patterns were developed in a 1:1 methyl isobutyl ketone (MIBK) - isopropanol (IPA) solution for 60 seconds, followed by an IPA rinse and N_2 drying. Metal deposition was carried out in a home-build UHV molecular beam epitaxy (MBE) setup, (base pressure $<1 \times 10^{-8}$ mbar), where a 5 nm titanium adhesion layer was deposited prior to a 30 nm gold layer, both at a rate of 0.5 Å/s as monitored by quartz crystal microbalance. Lift-off was performed by immersing the sample in acetone for 12 hours, followed by a brief (10 seconds) ultrasonic agitation and subsequent rinsing in IPA (60 seconds) before drying the surface by N_2.

Reflectance measurements were conducted using a FTIR spectroscopy (Bruker Vertex 80V) coupled with Hyperion 2000 microscope. All measurements were performed at room temperature under continuous N_2 purging to eliminate atmospheric absorption features. Spectra were acquired in the 6-12 μm (833-1667 cm^{-1}) spectral range with 4 cm^{-1} resolution. Reflectance values were normalized using a freshly deposited 100 nm gold mirror as reference. The incident angle was maintained at 15° relative to the surface normal to minimize detector saturation while ensuring sufficient signal intensity.

Electromagnetic simulations were performed using the FIT method in CST Studio Suite [24]. The computational domain implemented periodic boundary conditions in the x-y plane to model the infinite metamaterial array, with perfectly matched layers in the z-direction. For simplicity, in the simulations, a normal incident angle has been used instead of 15°, since the simulation results show negligible differences at small incident angles. Material properties were incorporated using standard optical constants for silicon and a Drude model for gold [18, 19]. The adaptive tetrahedral mesh was refined to $\lambda/50$ at the highest frequency to ensure convergence (<1% variation upon mesh doubling). Simulation reliability was validated through the reproduction of published cut-wire resonator results [18, 25].

The unit cell of the investigated metamaterial consists of two horizontally aligned parallel cut wires and a single orthogonally oriented crossed cut wire, all fabricated on a 800 μm-thick silicon substrate (Fig. 1). The horizontal cut-wires (HCW) are 1.3 μm long and 0.3 μm wide, while the vertical cut-wire (VCW) has a length of 1.2 μm and the same width. Initially, the crossed cut-wire was positioned at the center of the horizontal pair, but its location was systematically varied by introducing a lateral displacement d along the axis of symmetry. This parametric displacement was explored across multiple values ($d = 0$, 0.1, and 0.2 μm) to study the coupling influence on the electromagnetic response. Both numerical simulations and experimental measurements were conducted to analyze the spectral modifications induced by the structural asymmetry. The unit cell periodicity was fixed as 1.7 μm and 2.1 μm along x- and y-directions, respectively, to minimize near-field coupling between adjacent structures while ensuring a good far-field response.

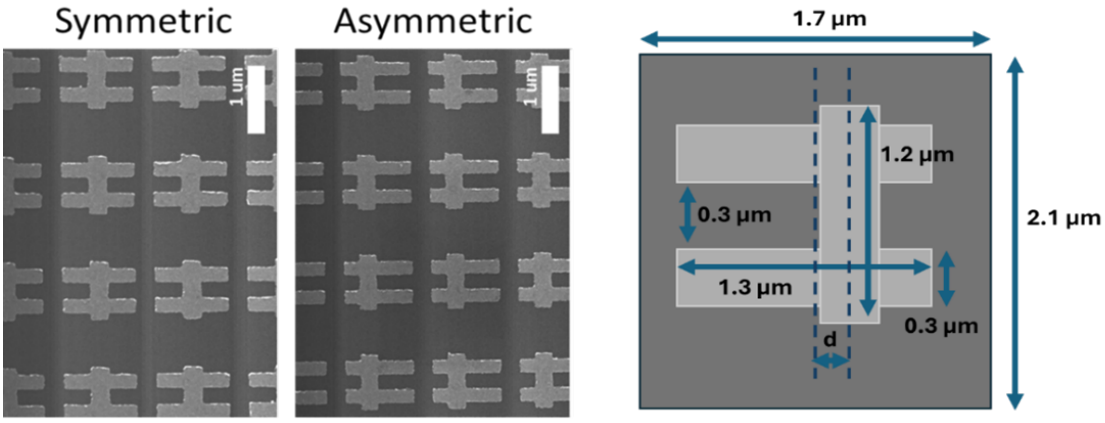

Fig. 1. SEM images of symmetric and asymmetric metamaterial samples and a sketch of the symmetric unit cell with the lateral displacement denoted as *d*.

3. Results and discussion

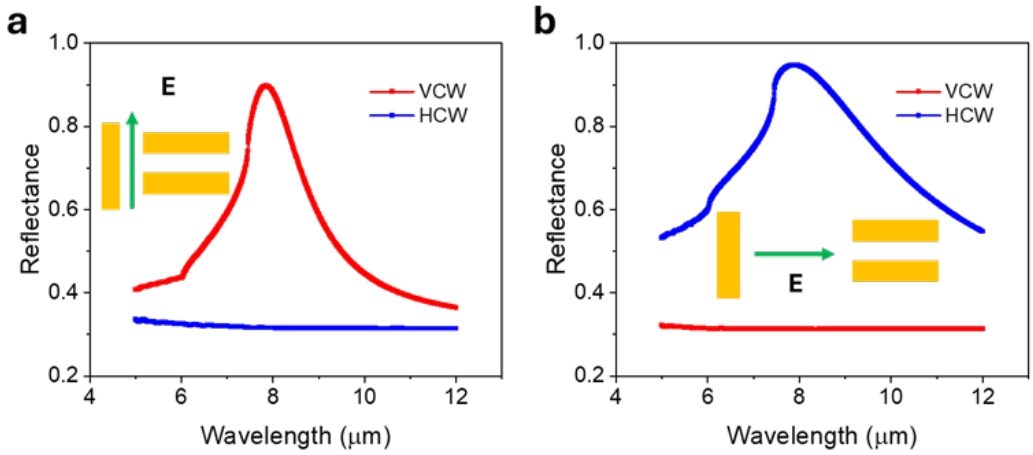

Fig. 2. (Color online) Simulated reflectance spectra of separated VCW (red) and HCW (blue) metamaterials at (a) the TE mode and (b) the TM mode at normal incident.

The HCW (1.3 μm) and VCW (1.2 μm) were designed with matched resonant wavelengths (~8 μm) to facilitate strong coupling. This near-degeneracy is critical for observing EIT, as it allows hybridization into symmetric and antisymmetric states, analogous to molecular orbital splitting [4]. The 0.1 μm length difference compensates for their distinct configurations (monomer for VCW and dimer for HCW), ensuring spectral overlap. Our experiments confirmed that under specific excitation conditions—either TE (Fig. 2a) or TM (Fig. 2b) polarization—only one of the resonators is excited. In the TE (TM) mode, the VCW (HCW) acts as the bright mode due to its strong coupling with the incident field, while the HCW (VCW) serves as the dark mode, weakly

radiative but capable of coupling with the bright mode. When combining VCW and HCW in the H-shaped configuration and breaking their symmetry, two hybridized modes are excited around the original resonance, resulting in a narrow transparency window and strong dispersion—hallmarks of EIT behavior as discussed below.

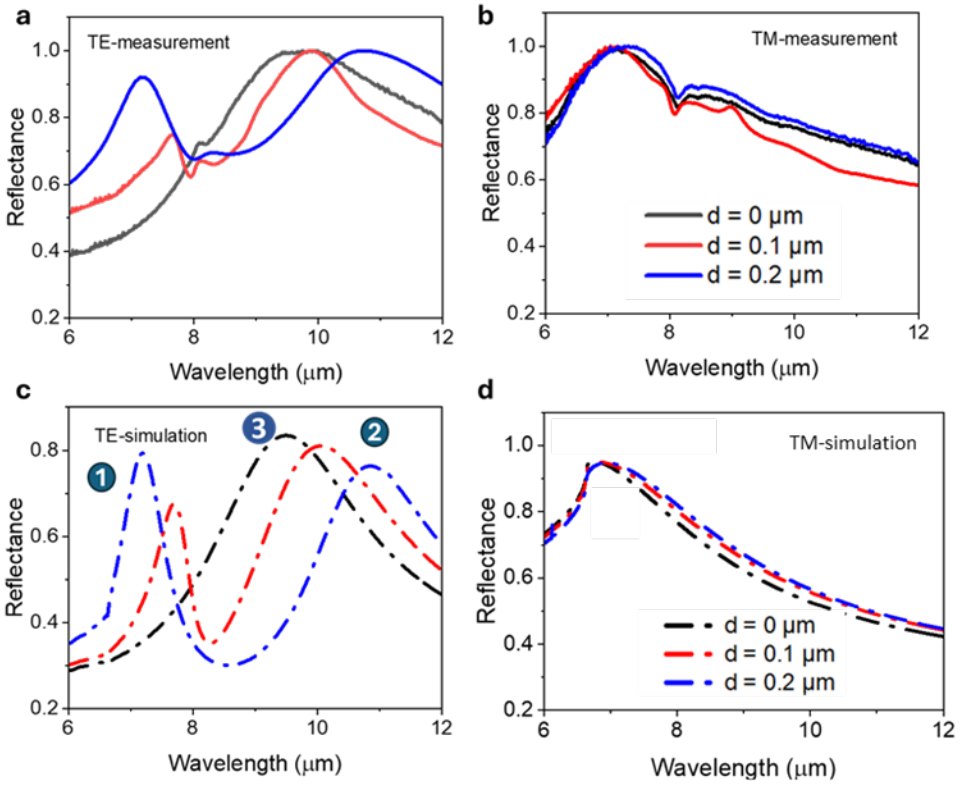

Fig. 3. (Color online) (a-b) Measured and (c-d) simulated reflectance of the EIT structure with different levels of asymmetry, with $d = 0$ μm (black), $d = 0.1$ μm (red), and $d = 0.2$ μm (blue) curves. The studied polarizations are TE and TM, as mentioned inside each figure panel, with the electric field polarizations pointing toward the VCW and HCW, respectively. The incident angles are 15° for the measurements and 0° for simulations.

Figure 3 presents measured and simulated reflectance spectra of EIT metamaterials for different levels of asymmetry in the 6–12 μm range under TE (Figs. 3a, 3c) and TM (Figs. 3b, 3d) polarizations. TE-polarized reflectance spectra show a clear evolution: from a single broad resonance at ~9.6 μm in the symmetric structure ($d = 0$ μm), to an EIT window at $d = 0.1$ μm, and finally to a well-defined and broader EIT window at $d = 0.2$ μm, with reflectance maxima at 47.0 μm and 10.8 μm. This spectral evolution and the broadening of the transparency window reflect the strengthening of mode hybridization between the bright VCW and dark HCW modes as the lateral displacement d increases [7]. The experiments show a decrease of the reflectance from 100% to 60%, i.e. 40% reflectance suppression, closely matching the 50% predicted by

simulations at $d = 0.2\ \mu$m. It is seen that the high refractive index of silicon sets a high reflection baseline, limiting the maximum achievable suppression in a single pass. Intrinsic absorption in the gold nanostructures, particularly in the narrow quadrupole antenna, dampens the sharpness and depth of the EIT resonance. Slight practical deviations from the designed geometry, especially for the small displacements, can blur the sharp resonance, reducing the quality factor and depth of the transparency window. The good agreement between experimental and simulated reflectance spectra validates the theoretical model and demonstrates the design's potential for tunable mid-infrared photonic applications.

In contrast, under TM polarization (Figs. 3b, 3d) all spectra exhibit a single resonance at ~7.0 μm, attributed to the HCW plasmonic mode. The sharp dip around ~8.0 μm seen in all experiments originates from an infrared absorption by silicon for the TM mode. TM-polarized excitation fails to induce strong coupling because the VCW's orientation renders it a dark mode. This polarization selectivity arises from the mismatch between the incident field vector and the VCW dipole moment, preventing energy transfer to the HCW. The resulting single resonance at ~7.0 μm mirrors the uncoupled HCW response, confirming the critical role of dipole alignment in plasmonic hybridization.

Further investigation into structural asymmetry is presented in Fig. 4, where the displacement parameter d is varied from 0 to 0.5 μm in steps of 0.025 μm. This analysis confirms the splitting behavior of the H-shaped structure under TE polarization and the symmetry-protected nature of the TM mode. As shown in Fig. 4a, the resonance splitting becomes more pronounced with increasing asymmetry. In contrast, the TM mode resonance remains at a constant wavelength but exhibits slight broadening as the metamaterial becomes more asymmetric.

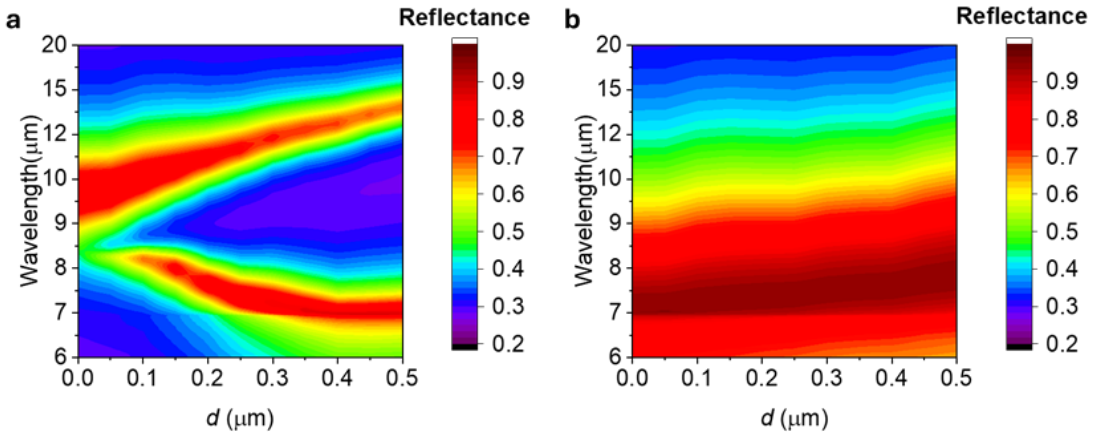

Fig. 4. (Color online) Extended simulation on reflectance of EIT metamaterials as function of d, varying from 0 to 0.5 μm for (a) TE mode and (b) TM mode.

Electric field profiles at key wavelengths in Fig. 5 reveal the underlying physics: (1,2) hybridized mode activation in the asymmetric HCW pair and (3) bright mode excitation along the VCW at 9.6 μm, leading to field suppression within the transparency window. The observed resonance splitting (~2.0 μm, from 7.6 μm to 9.6 μm) and strong field enhancement at the HCW edges confirm efficient plasmonic coupling. This behavior results from symmetry breaking,

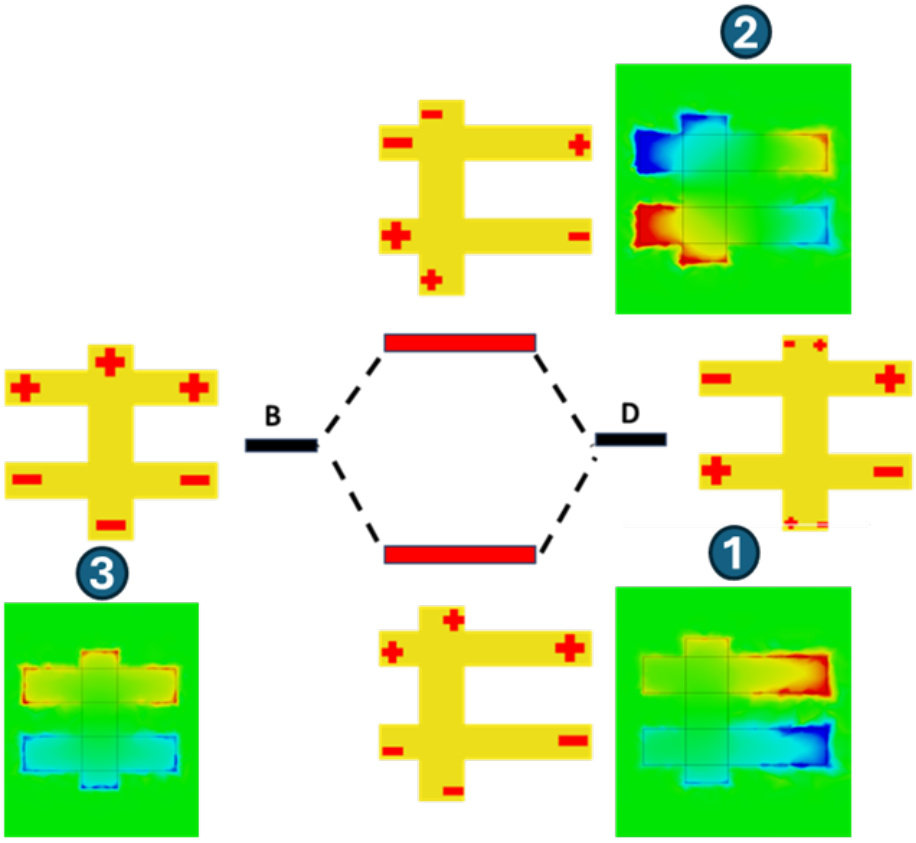

Fig. 5. Simulated electric field distributions at different resonant frequencies according to spectral positions (1), (2), and (3), corresponding to the wavelengths of 7 μm, 10.8 μm, and 9.6 μm, respectively, in Fig. 3c.

which enables strong coupling between the bright (VCW) and dark (HCW) modes. The resulting quadrupole mode (D-state) hybridizes with the dipole mode (B-state), forming two new resonant states with different frequencies and distinguishable electric field distributions.

The mismatch in reflectance amplitude and peak positions in reflectance spectra between simulation and experiments is investigated by simulating H-shaped metamaterials (for d = 0.2 μm) with a slight variation of geometrical parameters, including l_1, l_2, the lengths of vertical and horizontal antennas, and w, the width of all antennas. In each case, all other parameters except the investigated one are kept constant. Fig. 6 presents the shifts in the spectral position of the first peak, the middle of the EIT window, and the second peak with the variation of those geometrical parameters. As can be seen, the change of l_2 causes the largest spectral shift. Among the investigated parameters, only this dimension is changed in response to the asymmetry direction. There also is a blue shift of the second peak following the increase of w, which makes the coupling between the two horizontal bars of HPA stronger. This blueshift with the increase of w may also explain the main difference between experiment and simulation in Figs. 3a and 3b. Other

parameters impose negligible spectral shifts, demonstrating our structure as being spectral robust to slight deviations of geometrical parameters. SEM images from Fig. 1 show that the fabrication tolerance is below 5%, corresponding to approximately 3% of spectral shift from the simulation of Fig. 6.

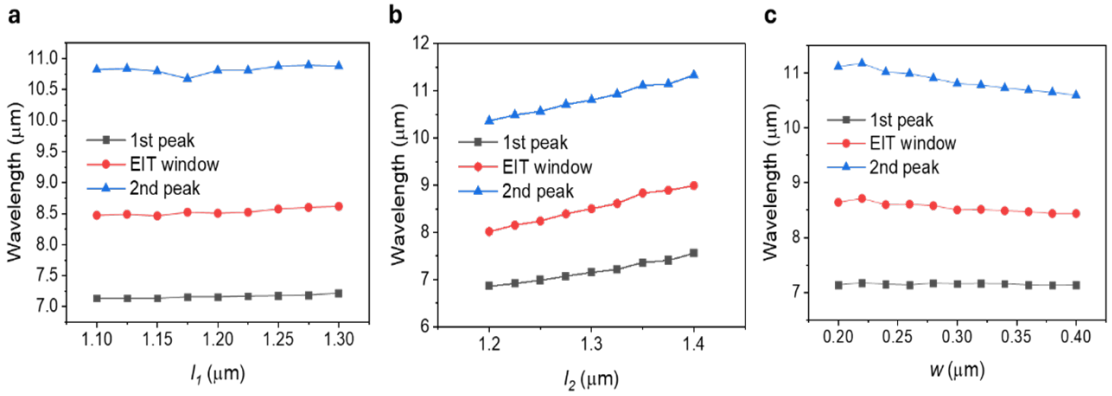

Fig. 6. The peak position of the first reflection peak, the middle of the EIT window, and the second reflection peak as a function of (a) l_1, (b) l_2, and (c) w, extracted from the simulation.

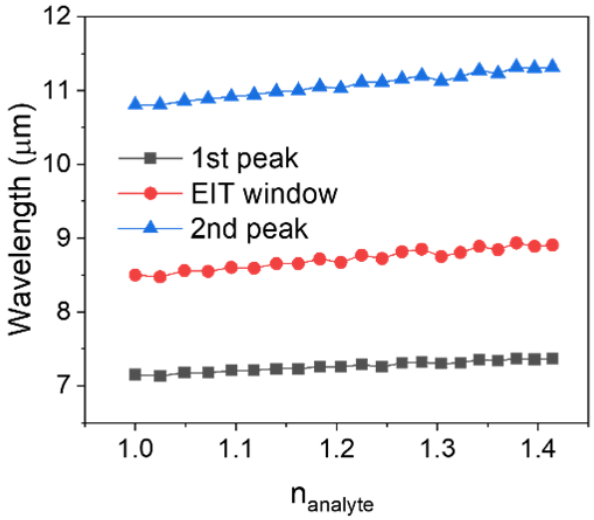

Fig. 7. The peak position of the first reflection peak, the middle of the EIT window, and the second reflection peak as a function of simulated analyte refractive index.

Finally, we investigate the sensitivity of H-shaped metamaterials to the refractive index change of the surrounding medium. This factor is particularly useful when utilizing this platform for optical sensing applications. Here, we calculate the spectral shift versus the refractive index

change, in units of nm/RIU, as shown in Fig. 7. Among the recorded peak positions, the first reflection peak shows a modest shift of 520 nm/RIU, while the middle of the EIT window and the second reflection peak exhibit larger shifts of 980 nm/RIU and 1240 nm/RIU, respectively. This value is about 4 THz/RIU, which is higher than those reported in several earlier works [26–28] and of the same order of magnitude as another study [29].

4. Conclusion

We have investigated the polarization-selective EIT effects through controlled symmetry breaking in H-shaped metamaterials, demonstrating the possibility to manipulate light-matter interactions at mid-IR frequencies. The observed anti-crossing behavior and hybridized mode dispersion establish that strong coupling persists in the mid-IR regime despite increased Ohmic losses. The displacement-dependent tuning of the transparency window suggests mechanical reconfigurability for dynamic devices. These findings address two fundamental challenges in infrared photonics: the spectral mismatch between molecular vibrations and plasmonic resonances, and the lack of polarization-selective components. The presented platform enables applications including: (i) enhanced molecular spectroscopy through polarization-multiplexed sensing, (ii) active optical elements with mechanical tuning, and (iii) quantum plasmonic systems leveraging mid-IR transitions. Future work may explore the integration with phase-change materials for non-mechanical tuning and coupling to quantum emitters for hybrid quantum-classical systems.

Acknowledgments

This work has been supported by a joint research project between the Research Foundation Flanders (FWO) under Grant G0DAX23N and the Vietnam National Foundation for Science and Technology Development (NAFOSTED) under Grant No. FWO.103-2022.01. T. L. P. acknowledges the KU Leuven Research Council for IRO scholarship ZB/21/023.

Authors contributions

The Linh Pham: Conceptualization, Investigation, Visualization, Writing (original draft). Nguyen Hai Anh and Nguyen Thi Mai: Investigation, Validation. Vu Dinh Lam: Validation, Writing (review). Nguyen Thanh Tung and Ewald Janssens: Conceptualization, Supervision, Validation, Funding acquisition, Resources, Writing (review & editing).

Conflict of interest

The authors have no conflict of interest to declare.

References

[1] S. A. Maier, *Plasmonics: Fundamentals and Applications*. Springer, 2007.
[2] J. B. Pendry, *Negative refraction makes a perfect lens*, Phys. Rev. Lett. **85** (2000) 3966.
[3] D. R. Smith, J. B. Pendry and M. C. K. Wiltshire, *Metamaterials and negative refractive index*, Science **305** (2004) 788.
[4] S. Zhang, D. A. Genov, Y. Wang, M. Liu and X. Zhang, *Plasmon-induced transparency in metamaterials*, Phys. Rev. Lett. **101** (2008) 047401.
[5] P. Tassin, L. Zhang, R. Zhao, A. Jain, T. Koschny and C. M. Soukoulis, *Electromagnetically induced transparency and absorption in metamaterials*, Phys. Rev. Lett. **109** (2012) 187401.

[6] M. Fleischhauer, A. Imamoglu and J. P. Marangos, *Electromagnetically induced transparency: Optics in coherent media*, Rev. Mod. Phys. **77** (2005) 633.
[7] N. Liu, L. Langguth, T. Weiss, J. Kastel, M. Fleischhauer, T. Pfau *et al.*, *Plasmonic analogue of electromagnetically induced transparency*, Nat. Mater. **8** (2009) 758.
[8] E. Prodan, C. Radloff, N. J. Halas and P. Nordlander, *A hybridization model for the plasmon response of complex nanostructures*, Science **302** (2003) 419.
[9] N. J. Halas, S. Lal, W.-S. Chang, S. Link and P. Nordlander, *Plasmons in strongly coupled metallic nanostructures*, Chem. Rev. **111** (2011) 3913.
[10] J. A. Fan, C. Wu, K. Bao, J. Bao, R. Bardhan, N. J. Halas *et al.*, *Self-assembled plasmonic nanoparticle clusters*, Science **328** (2010) 1135.
[11] A. Taflove and S. C. Hagness, *Computational Electrodynamics: The Finite-Difference Time-Domain Method*. Artech House, 2005, 10.1002/0471654507.eme123.
[12] F. H. L. Koppens, D. E. Chang and F. J. García de Abajo, *Graphene plasmonics: A platform for strong light-matter interactions*, Nano Lett. **11** (2011) 3370.
[13] P. Törmä and W. L. Barnes, *Strong coupling between surface plasmon polaritons and emitters*, Rep. Prog. Phys. **78** (2015) 013901.
[14] S. Law, D. C. Adams, A. M. Taylor and D. Wasserman, *Mid-infrared designer metals*, Opt. Express **20** (2012) 12155.
[15] N. Yu and F. Capasso, *Flat optics with designer metasurfaces*, Nat. Mater. **13** (2014) 139.
[16] F. Neubrech, C. Huck, K. Weber, A. Pucci and H. Giessen, *Surface-enhanced infrared spectroscopy using resonant nanoantennas*, Chem. Rev. **117** (2017) 5110.
[17] A. Boltasseva and H. A. Atwater, *Low-loss plasmonic metamaterials*, Science **331** (2011) 290.
[18] M. Bejide, A. Vantomme, N. T. Tung and E. Janssens, *Heat flow dynamics in planar metamaterials*, J. Phys. D: Appl. Phys. **55** (2022) 025105.
[19] F. Han, T. L. Pham, K. Pilarczyk, N. T. Tung, D. H. Le, G. A. E. Vandenbosch *et al.*, *Tunable mid-infrared multi-resonant graphene-metal hybrid metasurfaces*, Adv. Opt. Mater. **12** (2024) 2303085.
[20] N. Papasimakis, V. A. Fedotov, N. I. Zheludev and S. L. Prosvirnin, *Metamaterial analog of electromagnetically induced transparency*, Phys. Rev. Lett. **101** (2008) 253903.
[21] V. T. T. Thuy, N. T. Tung, J. W. Park, V. D. Lam, Y. P. Lee and J. Y. Rhee, *Highly dispersive transparency in coupled metamaterials*, J. Opt. **12** (2010) 115102.
[22] S. Liu, Z. Xu, X. Yin and H. Zhao, *High-Q-value classical electromagnetically induced transparency*, J. Opt. Soc. Am. B **38** (2021) 1156.
[23] L. Fan, Y. Yu, C. Gao, X. Qu and C. Zhou, *Prediction of strong coupling in resonant perovskite metasurfaces by deep learning*, Opt. Lett. **49** (2024) 4318.
[24] Dassault Systèmes, "CST studio suite." Software, 2023.
[25] U. T. D. Thuy, N. T. Thuy, N. T. Tung, E. Janssens and N. Q. Liem, *Large-area cost-effective lithography-free infrared metasurface absorbers*, APL Mater. **7** (2019) 071102.
[26] A. Zhu, M. Zhang, W. Hou, L. Cheng, C. Hu and C. Xu, *High-sensitivity graphene metasurface based on plasmon-induced transparency*, Photonics **12** (2025) 218.
[27] C. Tan, S. Wang, S. Li, X. Liu, J. Wei, G. Zhang *et al.*, *Cancer diagnosis using terahertz-graphene-metasurface-based biosensor*, Nanomaterials **12** (2022) 3889.
[28] S. Ma, P. Zhang, X. Mi and H. Zhao, *Highly sensitive terahertz sensor based on graphene metamaterial absorber*, Opt. Commun. **528** (2022) 129021.
[29] C. Zhang, Q. Liu, X. Peng, Z. Ouyang and S. Shen, *Sensitive THz sensing based on fano resonance in all-polymeric Bloch surface wave structure*, Nanophotonics **10** (2021) 3879.